Materials Chemistry and Physics 190 (2017) 136–145

Contents lists available at ScienceDirect

Materials Chemistry and Physics

journal homepage: www.elsevier.com/locate/matchemphys

Corrosion resistance improvement of nitinol by anodisation in the presence of molybdate ions

M. Saugo [a], D.O. Flamini [a, *], G. Zampieri [b, c], S.B. Saidman [a]

[a] Instituto de Ingeniería Electroquímica y Corrosión (INIEC), Departamento de Ingeniería Química, Universidad Nacional del Sur, Av. Alem 1253, 8000 Bahía Blanca, Argentina
[b] Centro Atómico Bariloche, Comisión Nacional de Energía Atómica, Av. Bustillo 9500, 8400 San Carlos de Bariloche, Argentina
[c] Instituto Balseiro, Universidad Nacional de Cuyo, Av. Bustillo 9500, 8400 San Carlos de Bariloche, Argentina

HIGHLIGHTS

- NiTi alloy was anodised applying a low voltage in the presence of a MoO_4^{-2} solution.
- The formed oxides provided good corrosion protection to the substrate.
- The presence of Mo in the oxide film was confirmed by different techniques.
- The increase of the Ti/Ni ratio in the oxidised sample was key to protection.

ARTICLE INFO

Article history:
Received 9 November 2015
Received in revised form
21 December 2016
Accepted 7 January 2017
Available online 9 January 2017

Keywords:
Alloys
Biomaterials
Oxides
X-ray photoemission spectroscopy (XPS)
Corrosion

ABSTRACT

The corrosion behaviour of Nitinol (NiTi) alloy was studied in Ringer solution. In order to improve its corrosion resistance, protective films were formed on the NiTi surface by means of anodisation under potentiostatic or galvanostatic control in the presence of the corrosion inhibitor molybdate in alkaline and acidic solutions.

The anodisation process reduces considerably the Ni content and increases the Ti content in the oxide film, indicating that the Ti/Ni stoichiometry in the outermost surface is much higher than in pure NiTi. The titanium enrichment on the outermost surface as TiO_2 enhanced its anticorrosion performance, as was suggested by the decrease in the amount of Ni and Ti released in Ringer solution under open circuit potential (OCP) condition and under potentials where the bare substrate suffers pitting attack.

The best anodised film in terms of corrosion protection was obtained under potentiostatic condition in alkaline solution. The presence of oxidised molybdenum species in the oxide potentiostatically grown in alkaline solution, generates a corrosion protective film with a smoother and denser surface than other oxides formed in acidic solutions, without any defects like micro-cracks or pores.

1. Introduction

In the last few decades Nitinol (equiatomic Ni and Ti alloy (NiTi)) has been widely used in many medical devices such as stents and orthopaedic and dental implants. In spite of its remarkable properties, superelasticity or shape memory effects, a limitation of the alloy is the release of ions into the biological environment, particularly Ni ions [1]. Ni ions may generate allergenic, toxic and carcinogenic reactions in the human body. Then, it is necessary to modify the surface of the alloy in order to improve its corrosion resistance. In this regard, different kinds of surface treatments were proposed such as heat treatments, chemical etching, laser irradiation and ion implantation [2].

The growth of an oxide layer on NiTi alloy is also a surface modification technique to improve corrosion resistance. Anodisation is a simple and efficient low-temperature method. The process allows preparing the coating in a one-step method in a short time. The corrosion resistance of NiTi alloy in Hanks' solution was improved by anodisation in acetic acid [3–5], sulphuric acid [6] and acetate and borate buffers [7]. The ability of the formed oxide film to inhibit Ni diffusion depends on its composition, structure and thickness, among other properties. The influence of the oxide film

* Corresponding author.
E-mail address: dflamini@uns.edu.ar (D.O. Flamini).

http://dx.doi.org/10.1016/j.matchemphys.2017.01.017
0254-0584/

thickness is controversial. As opposed to the general idea that a thicker oxide layer would provide a better prevention against ion release, these films are more susceptible to present cracks which might accelerate the release [1].

Molybdate is a known corrosion inhibitor for different metallic materials [8,9]. The anion reduces the passivity current, extends the passive range and increases the pitting potential in chloride media [10]. The presence of different molybdenum species incorporated into the oxide film has been reported and several explanations for its inhibitory effect on corrosion have been proposed [11]. Moreover, considering biomedical applications, the anion presents low toxicity and environmental acceptability [12].

On the other hand, molybdenum was alloyed on NiTi alloy by the laser surface alloying technique. Molybdenum was chosen to be the alloying element because of its good biocompatibility and non-toxicity feature. Addition of Mo gives improved pitting corrosion resistance and diminishes Ni release in Hanks' solution [13].

The aim of the present research work was to develop a new method to protect NiTi alloy against corrosion. A low-voltage anodisation in molybdate solution is considered as an alternative process to protect the alloy.

2. Materials and methods

NiTi rods in the form of discs axially mounted in a Teflon holder were used as working electrodes (WE). The exposed area of the WE is 0.0962 cm^2 and its chemical composition (in wt. %) is: 55.8 Ni, 0.05 O, 0.02 C and Ti balance. Before each experiment, the WE was abraded with SiC papers down to 1200 grit finish, then degreased with acetone and finally washed with triply distilled water. Then, the WE was immediately transferred to an electrochemical cell. A large Pt sheet was used as counter electrode and a saturated calomel electrode (SCE) was used as reference electrode. All potential values in this work are referred to SCE. All electrochemical experiments were performed in a Metrohm cell of 20 cm^3 utilising a potentiostat-galvanostat PAR Model 273A.

The anodisation of the NiTi alloy was carried out potentiostatically and galvanostatically using a rotating disk electrode EDI 101 (Radiometer Analytical S.A.) with a CTV 101 rotation rate controller (Radiometer Analytical S.A.) in solutions with and without Na_2MoO_4. A 0.50 M Na_2MoO_4 was employed. The pH was adjusted to 2 or 12 by adding H_2SO_4 or NaOH, respectively. The corrosion performance of the coatings was evaluated by open circuit potential (OCP) value variation with time, linear sweep voltammetry (LSV) and potentiostatic measurements in Ringer solution: 0.147 M NaCl; 0.00432 M $CaCl_2$; 0.00404 M KCl, giving a total chloride concentration of 0.16 M [14]. All chemicals were reagent grade and solutions were made with triply distilled water.

Ni, Ti and Mo released concentrations in Ringer solution were analysed using an inductively coupled plasma atomic emission spectrometer (ICP-AES) (ICPE 9000 - Shimadzu Corporation, Japan).

A dual stage ISI DS 130 scanning electron microscopy (SEM) was used to examine the characteristics of the electrodes surface. To determine the qualitative composition of the oxide a MagiX X-Ray Fluorescence (XRF) spectrometer (PANalytical) was used. In this case, two different crystals were employed, LiF200 and PE, in a helium atmosphere and a Rh tube.

X-Ray photo-emission spectroscopy (XPS) was performed with a hemispherical electrostatic energy analyser (r = 100 mm) using Al K_α radiation ($h\nu$ = 1486.6 eV). The binding-energy (BE) scale was calibrated with $Au4f_{7/2}$ peak measured in a clean Au surface, placed at 84.0 eV. Depth profiling were performed with 2 keV Ar^+ ions incident at 60° from the surface normal; simulations made with the program TRIM [15] show that the sputtering yield under these conditions is S = 2.7, similar for both Ni and Ti; therefore, for the typical current densities used in the experiments (around 5 μA cm^{-2}) the sputtering rate was in the order of 1 nm min^{-1}.

3. Results and discussion

3.1. Anodisation process

The anodisation was conducted potentiostatically or galvanostatically during 1 h in a 0.50 M Na_2MoO_4 solution at different pH values (2 and 12). A rotating electrode was employed in order to avoid great oscillations in the transients due to the oxygen evolution, reaction that is produced simultaneously with the oxide growth. The rotation speed was 500 rpm in all cases. In order to choose the applied potential, some preliminary trials were carried out. Bare NiTi electrodes were anodised as it was previously detailed applying three different potentials: 1.0, 1.5 and 2.0 V (SCE). Then their corrosion performance was evaluated by means of variation of OCP with time and LSV measurements in Ringer solution. The best results were obtained for the sample anodised at 2.0 V(SCE). The transients obtained during the anodisation are shown in Fig. 1(A). It can be observed that a current density close to 70 mA cm^{-2} is reached, so this value was applied during galvanostatic anodisation in order to obtain a potential as near as possible to 2.0 V(SCE) (Fig. 1(B)). The steady state potential was reached in a few seconds and did not vary with time. This agrees with was reported by P. Shi et al. for NiTi alloy anodised in acetic acid [3]. Velten et al. had proposed for Ti and a Ti alloy that changes in the oxide structure from amorphous to crystalline were produced during progressive anodising. As a result of this behaviour, there is a change from ionic conductivity, which is necessary for the film growth, to electronic conductivity, where the growth is retarded and finally stops [16].

When the anodisation process was carried out whether galvanostatically or potentiostatically in acidic medium, the molybdate solution had a dark blue colour. This was because molybdates were present in a polymeric form and the anion $Mo_6O_2^{16-}$ became the dominant specie [17]. These complex anions form a solution of molybdenum blue, where Mo has a valence between V and VI [10].

Independently of the anodisation technique and the solution pH, all the electrodes presented a golden-coloured surface after they were removed from the electrochemical cell. This result was associated with the formation of an oxide layer composed of TiO_2 on the outermost surface, as was previously reported by other authors [18–20].

3.2. Corrosion protection

To determine if the formed oxide layers provide a good protection against corrosion to the NiTi alloy, several tests were carried out in Ringer solution. Fig. 2 exhibits the results of the OCP value versus time for the electrodes anodised in alkaline and acidic solutions during 1 h. In the case of the samples prepared in alkaline solution the highest increment in the OCP value was obtained for the sample anodised at 2.0 V (Fig. 2(A), curve b), while the samples prepared in acidic solution present a similar positive shift (Fig. 2(B), curves b and c).

The LSV tests performed are shown in Fig. 3. The abrupt increase of the current density denotes the breakdown of the passive layer (Fig. 3(A), curve a and c) [17]. The sample anodised potentiostatically in the pH 12 solution shows an important increment in the length of the passive zone (Fig. 3(A), curve b). Again, the samples prepared in the acidic solution have a similar behaviour, showing a positive shift in the pitting potential when they are compared to the bare NiTi alloy (Fig. 3(B)).

To determine if the presence of Mo in the oxide layer influenced

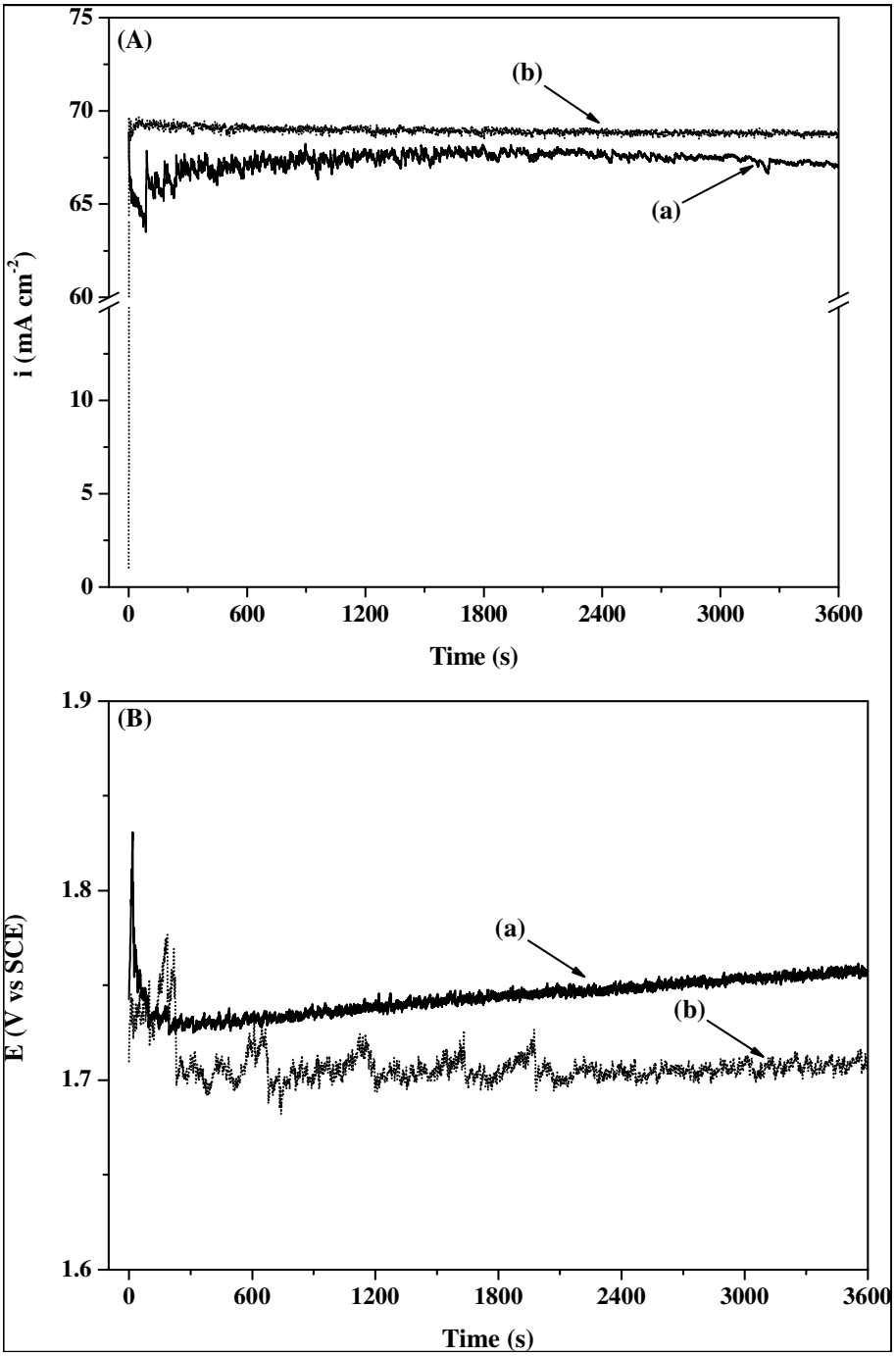

Fig. 1. Anodisation of NiTi alloy at: (A) 2.0 V and (B) 70 mA cm^{-2} during 1 h in a 0.50 M Na_2MoO_4 solution. In both cases the WE was rotated at 500 rpm and pH values were: (a) 12 and (b) 2.

the anticorrosion properties, the anodisation was performed at 2.0 V(ECS) during 1 h at 500 rpm in molybdate-free alkaline (pH 12) and acidic (pH 2) solutions. The anodised samples obtained in the absence of molybdate behave similarly to the bare NiTi alloy when a LSV was carried out (results not shown), indicating that molybdenum species were incorporated into the oxide layer playing an important role in the protection of the substrate.

The variation of OCP value as a function of time during long periods in an aggressive medium can be used to evaluate the protection degree of the covered substrate. In this case, the samples anodised potentiostatically at pH 2 and 12 were immersed in Ringer solution during one week and their OCP was monitored. These samples were chosen because the oxide films formed on NiTi alloy under these conditions presented the best pitting corrosion resistance with respect to the oxide formed under galvanostatic conditions. The obtained values are displayed in Fig. 4 and compared to the result corresponding to the bare NiTi alloy. As it can be observed, both anodised electrodes keep a positive value of the OCP even after one week of immersion. The remaining solutions were analysed by ICP-AES and the presence of Ni, Ti and Mo were determined (Table 1). The amount of released Ni, which is the major concern, diminishes considerably when NiTi alloy is previously

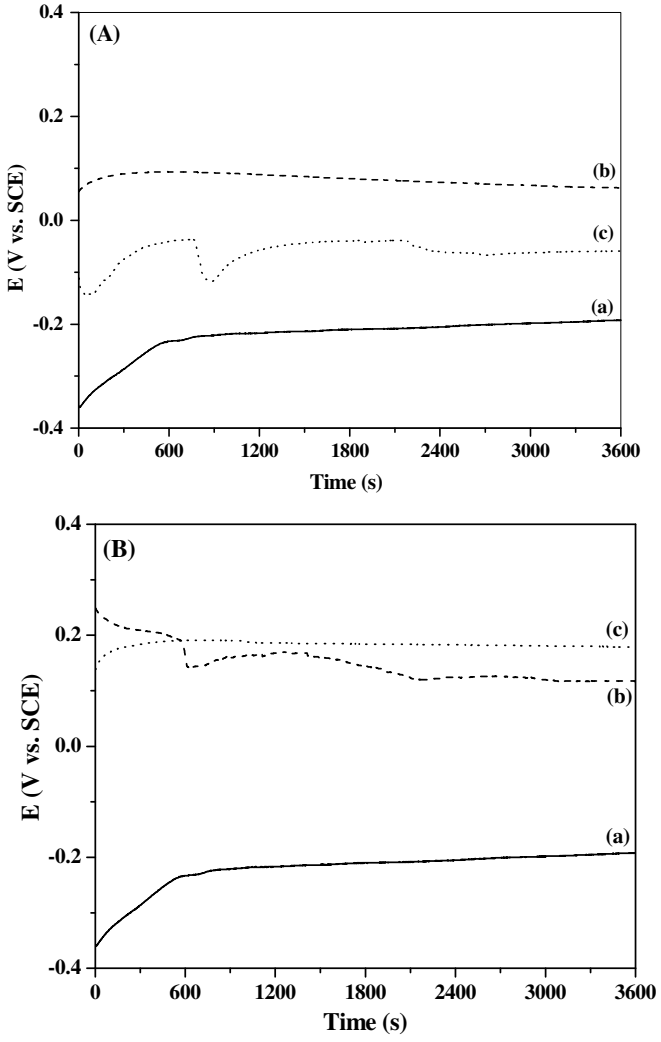

Fig. 2. OCP vs. time in Ringer solution for: (a) bare NiTi alloy, (b) NiTi alloy anodised at 2.0 V during 1 h at 500 rpm, (c) NiTi alloy anodised at 70 mA cm^{-2} during 1 h at 500 rpm. A 0.50 M Na_2MoO_4 solution was used during anodisation at different pH values: (A) 12 and (B) 2.

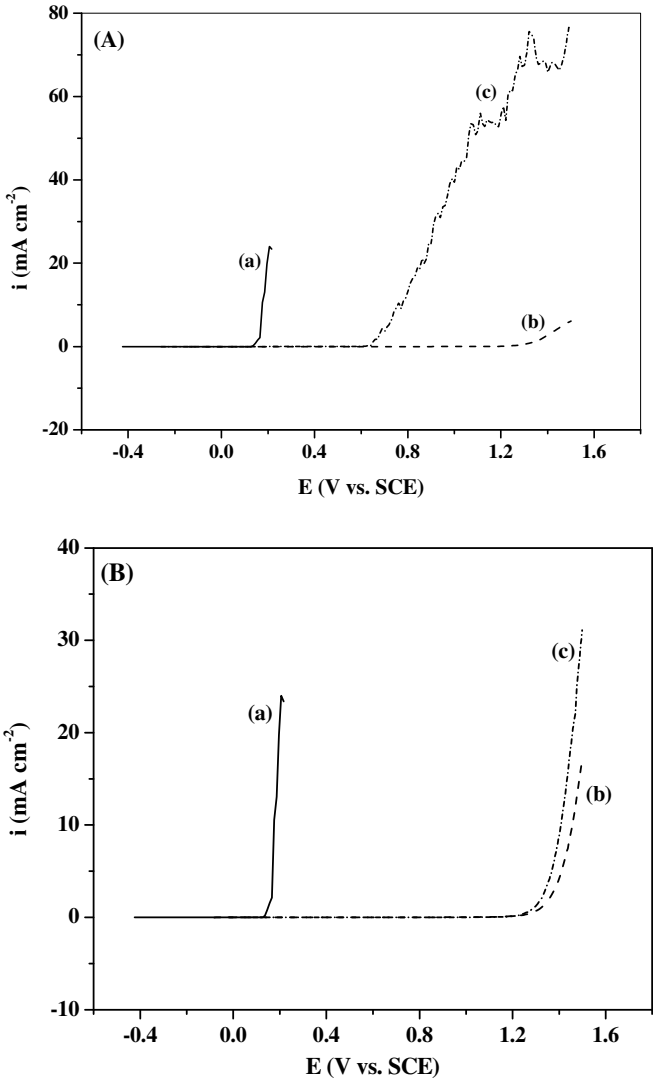

Fig. 3. LSV at 10 mV min^{-1} in Ringer solution for: (a) bare NiTi alloy; (b) NiTi alloy anodised at 2.0 V during 1 h at 500 rpm (c) NiTi alloy anodised at 70 mA cm^{-2} during 1 h at 500 rpm. A 0.50 M Na_2MoO_4 solution was used during anodisation at different pH values: (A) 12 and (B) 2.

anodised. The presence of Mo in the oxide layer was confirmed given that this element was found in the Ringer solution where each anodised samples was immersed.

In order to check the protection level under more drastic conditions the current density-time response was registered for bare and anodised NiTi alloy in Ringer solution at a potential more positive than the one corresponding to the pitting potential of the bare sample (0.65 V (SCE)) (Fig. 5). After 1800 s of polarisation, a high current density value was measured (60 mA cm^{-2}) for bare NiTi alloy which indicates that localised corrosion of the sample is developed (Fig. 5, curve a). As it can be seen in curve b of Fig. 5, the current density value measured for anodised NiTi alloy after applying a constant potential value of 0.65 V(SCE) during 8 h in Ringer solution was 0.01 mA cm^{-2}. This current density value is significantly lower than that for the bare NiTi alloy, which indicates that the oxide grown potentiostatically in alkaline solution is a protective film. The ICP-AES analysis of the amount of Ni, Ti and Mo released into the Ringer solution are presented in Table 2. The data confirmed that the dissolution of the alloy was significantly reduced by the presence of the anodised oxide film formed in the alkaline molybdate solution.

According to the previously obtained results, only the NiTi alloy anodised in the alkaline molybdate solution under potentiostatic control was considered for further characterisation.

3.3. Film characterisation

3.3.1. SEM measurements

A SEM analysis was performed to determine the surface characteristics of the anodised electrodes. The sample anodised potentiostatically in a pH 12 MoO_4^{2-} solution was characterised on account of the previous experiments, given that the oxide formed under these conditions provides anodic protection to the NiTi alloy and it also protects the substrate against pitting corrosion. To the naked eye, the formed oxide layer is smooth and compact. The SEM images presented in Fig. 6 show that the surface of the film formed without rotation (Fig. 6(a)) is rougher than the one formed with the rotating electrode (Fig. 6(b)). This could be because, in the first case, the O_2 bubbles formed were retained on the surface of the electrode. The fact that the oxide layer formed in the presence of molybdate is not porous and does not present any cracks is

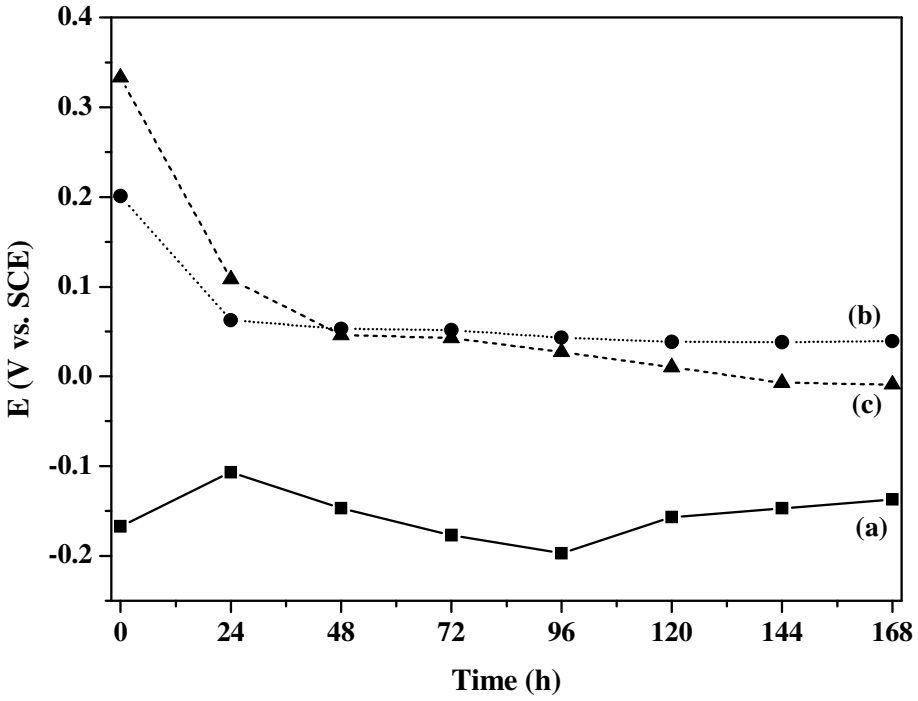

Fig. 4. Time dependence of the OCP in Ringer solution of: (a) bare NiTi alloy, NiTi alloy anodised at 2.0 V during 1 h at 500 rpm in a 0.50 M Na_2MoO_4 solution at (b) pH 12 and (c) pH 2.

Table 1
Concentration of Ni, Ti and Mo released after OCP in Ringer solution for bare NiTi alloy and different anodised samples: NiTi alloy anodised at 2.0 V during 1 h at 500 rpm in a 0.50 M Na_2MoO_4 solution at (a) pH 12 and (b) pH 2.

Sample	Ni concentration (mg L^{-1})	Ti concentration (mg L^{-1})	Mo concentration (mg L^{-1})
Bare NiTi	2.34	<0.05	<0.05
Anodised NiTi (a)	<0.05	<0.05	0.065
Anodised NiTi (b)	<0.05	<0.05	0.132

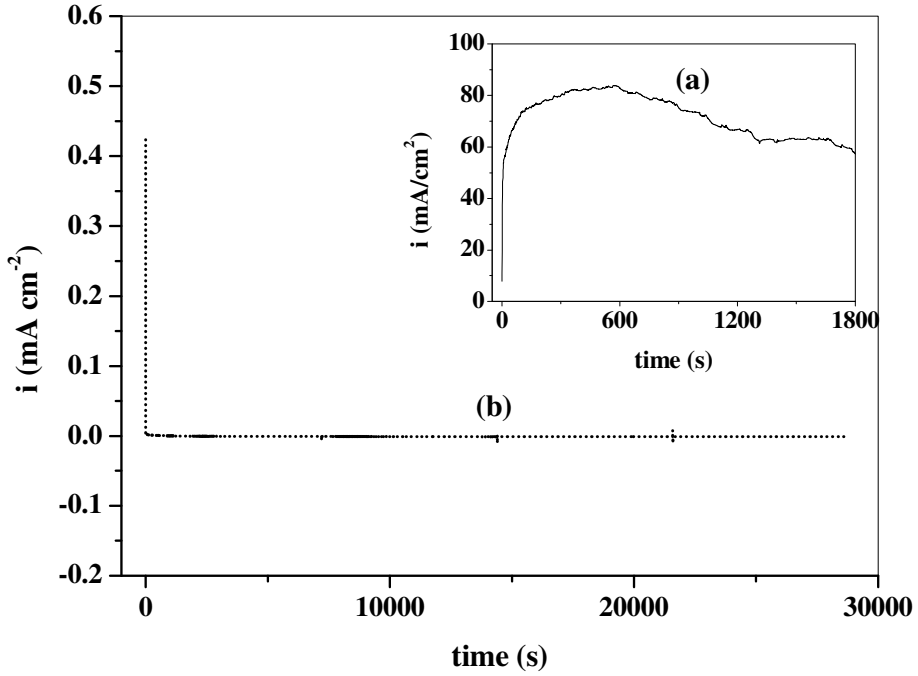

Fig. 5. Potentiostatic response obtained at 0.65 V(SCE) in Ringer solution for: (a) bare NiTi alloy and (b) NiTi alloy anodised at 2.0 V during 1 h at 500 rpm in a 0.50 M Na_2MoO_4 solution at pH 12.

Table 2
Concentration of Ni, Ti and Mo released after anodic polarisation in Ringer solution for bare NiTi alloy and the anodised sample. (*) NiTi alloy was anodised at 2.0 V during 1 h at 500 rpm in a 0.50 M Na_2MoO_4 solution at pH 12.

Sample	Applied potential (V vs. SCE)	Time (h)	Ni concentration (mg L^{-1})	Ti concentration (mg L^{-1})	Mo concentration (mg L^{-1})
Blank	–	–	0.015	<0.002	<0.05
Bare NiTi	0.65	0.5	20.3	1.17	<0.05
Anodised NiTi (*)	0.65	8	<0.05	<0.05	0.355

consistent with the data found in the literature [18].

3.3.2. XRF

A useful technique to determine if Mo is present in the oxide layer is XRF, which is non-destructive and non-invasive. The spectra obtained are displayed in Fig. 7. The K_α and K_β signals of Ni and Ti correspond to the NiTi alloy (Fig. 7(A)). The Rh signals originate from the excitation source. The Ca and P signals correspond to the sample holder while the Cl, Si and Al are contaminants from the rinse or the abrading procedure. In Fig. 7(B), the peaks corresponding to Mo L_α and L_β can be observed, which indicates that this element is present in the oxide layer. For further information about the amount of Mo or its oxidation state other techniques are necessary.

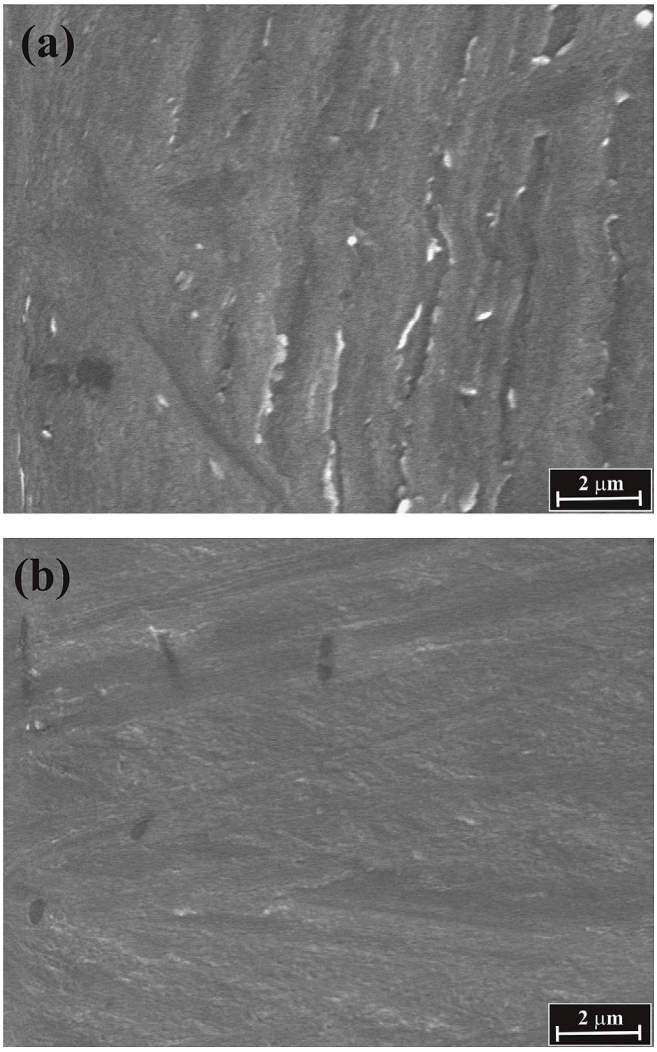

Fig. 6. SEM images of the oxide layer formed potentiostatically on NiTi alloy at 2.0 V during 1 h in a 0.50 M Na_2MoO_4 solution at pH 12: (a) without rotation and (b) rotating at 500 rpm.

3.3.3. XPS

An XPS analysis was performed to bare NiTi alloy and to the sample anodised potentiostatically in a MoO_4^{2-} solution of pH 12.

Fig. 8 shows the evolution with the sputtering cycles of the most prominent peaks in the photoemission of both samples. The Ar doses have been converted into removed thickness using a sputtering yield S = 2.7, and the depths corresponding to each set of spectra are listed on the right (the sputtering yield was calculated with the program SRIM [15] using parameters for pure NiTi alloy). The initial spectra of bare NiTi alloy (Fig. 8(a)) shows an important presence of O in the surface region. In spite of that fact, the position of the $Ni2p_{3/2}$ peak indicates that Ni is in the metallic state. On the contrary, the position of the $Ti2p_{3/2}$ peak almost coincides with its position in TiO_2 thereby indicating that Ti is mostly oxidised. In the spectra taken at a depth of 8 nm the O1s peak has decreased markedly and the $Ti2p_{3/2}$ peak has shifted to the position of metallic Ti. After this change the sputtering produces only a gradual disappearance of the O1s peak, without much modification of Ni2p and Ti2p peaks.

The initial spectra of the anodised sample (Fig. 8(b)) show a situation in the surface region similar to the one found for bare NiTi alloy. The prominent O1s peak reveals an important presence of O and the positions of the Ni2p and Ti2p peaks show that only Ti is oxidised. In effect, while the $Ti2p_{3/2}$ peak appears at 458.4 eV, which is 4.3 eV shifted from the position of metallic Ti and almost in coincidence with the position in TiO_2, the $Ni2p_{3/2}$ peak appears at 853.0 eV, which is very close to the position in metallic Ni. A closer analysis shows the existence of a minor component at about 856 eV, which, however, does not correspond to NiO because in this compound the $Ni2p_{3/2}$ peak is expected at 853.8 eV.

The evolution of the spectra with the sputtering is quite different from that observed in the bare NiTi alloy. The spectra remain relatively stable up to a depth between 40 and 50 nm, showing only a gradual increase of the relative intensity of the peak $Ni2p_{3/2}$ with respect to the intensities of O1s and $Ti2p_{3/2}$ peaks. From this depth on, the O1s peak decreases steadily and, in the case of the $Ti2p_{3/2}$ spectrum, the metallic component begins to grow at the expense of the oxidised one. At a depth of about 120 nm a situation similar to that found at the end of the depth profiling of the bare NiTi is reached. Fig. 8(b) also shows the evolution of the Mo3d spectrum during the sputtering; it is seen that Mo is concentrated in the region between 10 and 60 nm. According to the thickness removed by the Ar bombardment during XPS measurements, the thickness of the natural oxide layer formed on the bare NiTi alloy and the oxide grown by anodisation can be estimated in 35 and 120 nm, respectively.

Fig. 9 compares the spectra at two stages of the depth profiling of the anodised sample. Panels (a) and (b) represent the situations at the outermost and inner surface of anodised NiTi alloy, respectively. The comparison evidences three important differences: i) the presence of O in the outermost surface; ii) that Ti is almost completely oxidised in the outermost surface and in metallic state in the inner surface, and iii) the stoichiometry of Ni and Ti in the outermost surface is different from that in the substrate, existing an important enrichment of Ti.

To advance in the analysis all the spectra of the anodised sample

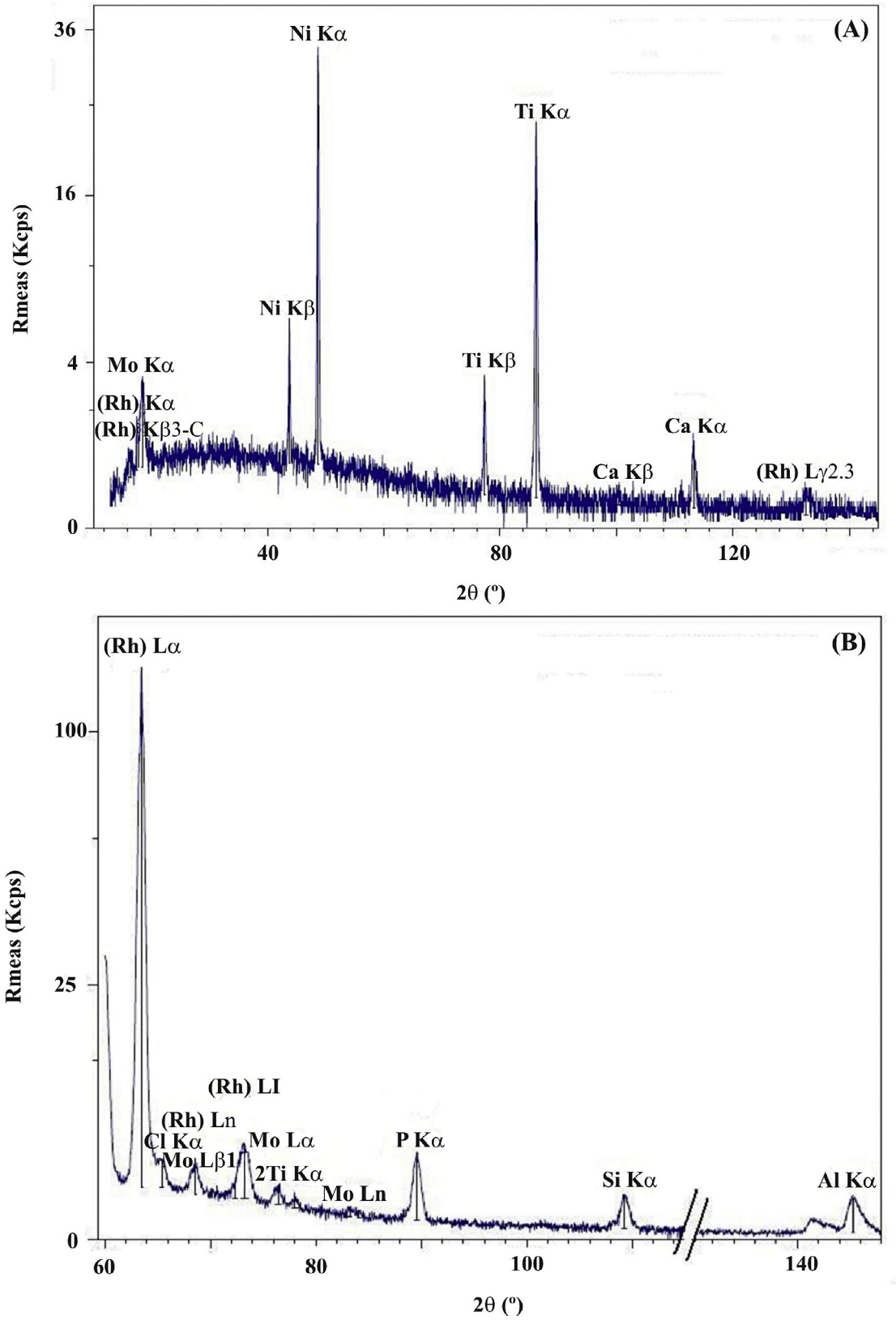

Fig. 7. XRF spectra of NiTi alloy anodised at 2.0 V during 1 h at 500 rpm in a 0.50 M Na_2MoO_4 solution at pH 12. Two crystals were used: (A) LiF200 and (B) PE.

were fitted. The fitting curves are shown in Figs. 8(b) and 9 superimposed on the measured spectra. The latter figure also shows the elemental components used in each case. All the fittings were made with Doniach-Sunjic functions and a linear background with a Shirley-type step. In the case of the $Ni2p_{3/2}$ spectra two components were used to give account of the main peak and the minor component and a third much broader component to give account of the satellite present at about 8 eV from the main peak.

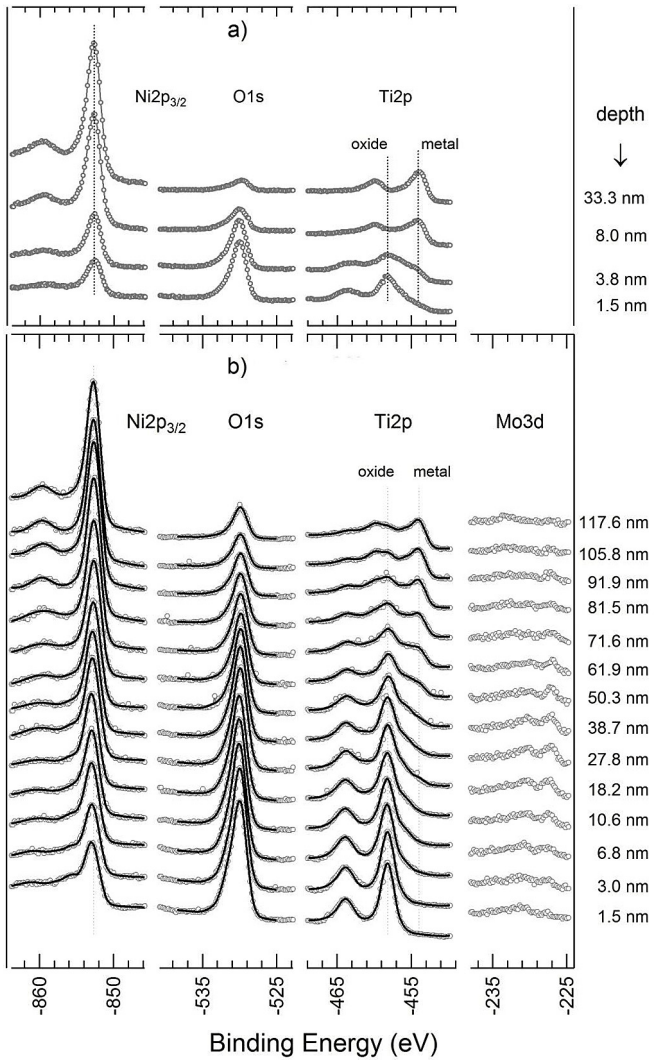

Fig. 8. $Ni2p_{3/2}$, O1s, Ti2p and Mo3d core-level spectra acquired during the depth profiling (the intensities of the Mo3d spectra shown are multiplied by 5). The numbers on the right indicate the thickness removed by the Ar bombardment. The black lines on the spectra of panel (b) are fitting curves obtained as explained in the text. Panel (a): bare NiTi alloy and panel (b): NiTi alloy anodised at 2.0 V during 1 h at 500 rpm in a 0.50 M Na_2MoO_4solution at pH 12.

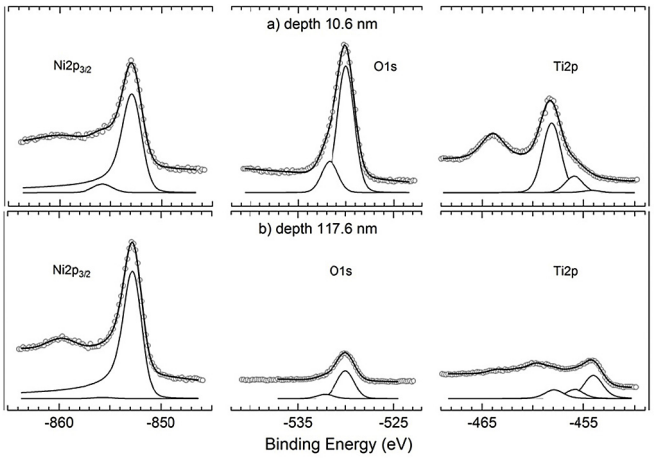

Fig. 9. Comparison of the $Ni2p_{3/2}$, O1s and Ti2p spectra of the anodised sample (NiTi alloy anodised at 2.0 V during 1 h at 500 rpm in a 0.50 M Na_2MoO_4 solution at pH 12) at two stages of the depth profiling. The best fitting curves are shown superimposed on the spectra and the main components used in each fitting are shown under the spectra.

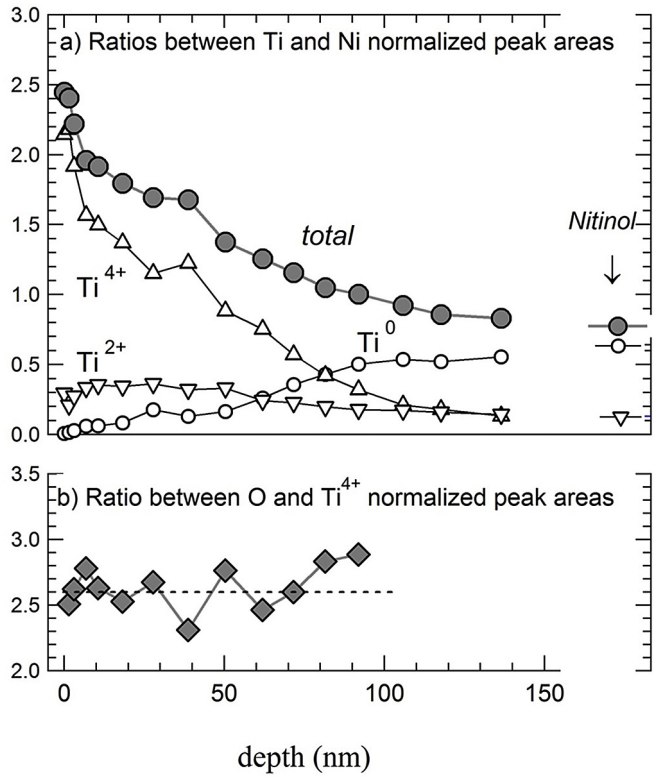

Fig. 10. Ratios between peak areas normalised with the photoionisation cross sections. (a) Ratios between the areas of the three components of the Ti2p spectrum and the metallic component of the Ni2p spectrum. (b) Ratio between the area of the main component of the O1s peak and the Ti^{4+} component of the Ti2p spectrum.

The Lorentzian width of the first two components was set at 0.25 eV while the asymmetry parameters were set at 0.16 and 0 for the main (metallic) and minor components, respectively. The O1s spectra were fitted with three components of the same line shape, with Lorentzian width 0.2 eV and zero asymmetry. Finally, the Ti2p spectra were fitted with three $2p_{1/2,3/2}$ spin-orbit doublets made of two identical peaks separated by 5.6 eV and fixed 1:2 intensity ratio. The Lorentzian widths were set at 0.2 eV for the three components and the asymmetry parameters were 0.12 for the lowest binding-energy component (metallic) and 0 for the other two. The Gaussian widths and the intensities were left free in all the fittings. With regards to the positions, in the $Ni2p_{3/2}$ and O1s spectra the positions of the main components were left free and the separations of the minor components were optimised in the first spectra and thereof kept fixed; in the $Ni2p_{3/2}$ spectrum the separation was fixed at 3.0 eV (the position of the satellite was left free) and in the O1s spectrum the separations were fixed at 1.7 and 3.6 eV, respectively. In the case of the Ti2p spectrum the components at the low and high binding-energy sides were fixed at 454.1 eV and 458.3 eV, respectively, and the position of the component in the middle of these two was left free. Then, using the intensities, Gaussian widths and some positions as free parameters all the $Ni2p_{3/2}$, O1s and Ti2p spectra were fitted, obtaining an excellent agreement in all cases. The positions of the $Ni2p_{3/2}$ and O1s main components were 852.7 ± 0.1 and 530 ± 0.1 eV, respectively, which coincide with the positions reported for metallic Ni and TiO_2 [21]. The position of the component that was left free in the fitting of the Ti2p spectra was stable at 456.0 eV within ±0.2 eV; therefore, the

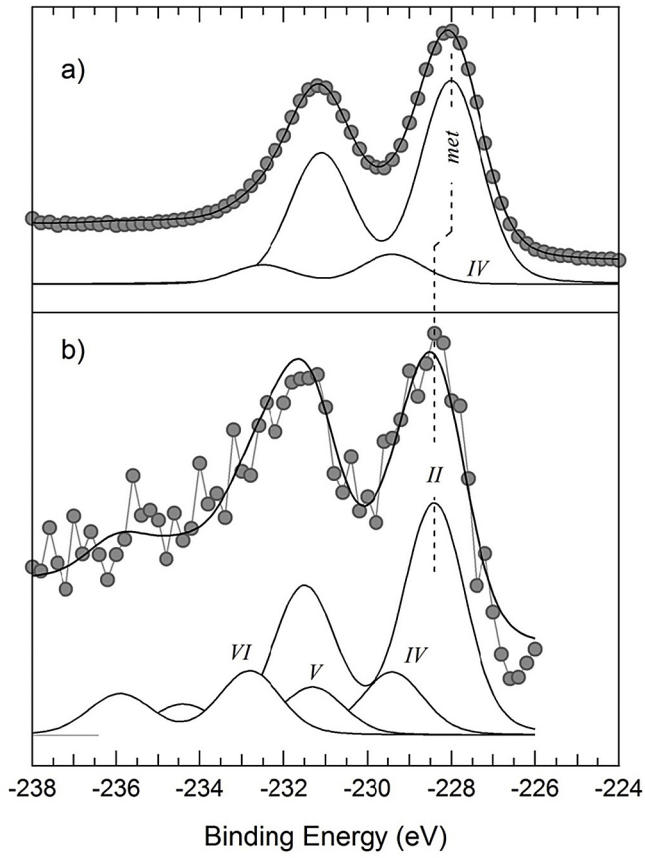

Fig. 11. Comparison of Mo3d spectra acquired in: (a) metallic Mo and (b) anodised sample (NiTi alloy anodised at 2.0 V during 1 h at 500 rpm in a 0.50 M Na_2MoO_4 solution at pH 12) at a depth of 27.6 nm. The black lines are the best fitting curves and the most important components used in each case.

three components of the Ti2p spectrum are identified as follows: the components at 454.1 and 458.3 eV are assigned to metallic Ti and TiO_2, respectively and the component at 456.0 eV to an intermediate oxide (TiO) [21]. In what follows these three components will be referred to as Ti^0, Ti^{2+} and Ti^{4+} in order of increasing binding energy.

Fig. 10 presents some intensity ratios made with the results obtained in the fittings. The peak intensities have been divided by the corresponding photoionisation cross sections [22] to approximately represent ratios between atomic concentrations. The ratios between the intensities of the Ti2p components and the metallic component of the Ni2p spectra are presented in Fig. 10(a) and show several interesting aspects. First, it is seen that in the outermost surface Ti is mainly as Ti^{4+}. Second, the presence of Ti^0 in the first part of this region is negligible, but then it increases continuously and between 70 and 80 nm becomes the dominant component. Third, at a depth of around 120 nm all the intensity ratios have reached the values obtained in pure NiTi alloy, and thence this depth may be taken as the end of the treated region. Finally, it is seen that the Ti/Ni stoichiometry in the outermost surface is much higher than in pure NiTi. This result constitutes a comparative advantage for future applications because the Ni content of the anodised oxide film is reduced considerably.

Fig. 10(b) presents the intensity ratio between the main component of the O1s peak and the Ti^{4+} component. It is seen that this ratio is relatively stable around 2.6 in the whole outermost surface, what is taken as strong evidence that the O present in this region is mostly bonded to Ti forming TiO_2.

Finally, Fig. 11 presents a comparison of the Mo3d spectra of the anodised sample at a depth of 26.7 nm with that of metallic Mo. The reference spectrum of Fig. 11(a) shows two peaks separated by 3.1 eV which correspond to the $3d_{3/2}$ and $3d_{5/2}$ spin-orbit split core levels. The spectrum in Fig. 11(b) shows a slight shift to larger binding energies and a $3d_{3/2}$ peak bigger and broader than in (a); both changes denote the existence of oxidised species. Both spectra of Fig. 11 were fitted with 5 elemental components with relative separations as reported in Ref. [23]. The component at the lowest binding energy is assigned to metallic Mo and the components at 1.4 and 4.8 eV larger binding energies to the stoichiometric oxides MoO_2 and MoO_3, which are designated Mo(IV) and Mo(VI), respectively; the other two components at 0.4 and 3.3 eV are ascribed to non-stoichiometric oxides and are designated Mo(II) and Mo(V), respectively. The fitting of the spectrum in Fig. 11(a) yields a dominant metallic component and a small Mo(IV) component. In the case of the Mo3d spectrum of the anodised sample the fitting shows a prevalence of the oxidised species, with a negligible contribution of the metallic component.

4. Conclusions

The corrosion behaviour of bare NiTi alloy in chloride solution is principally related to a selective dissolution of nickel element present in the natural oxide. An anodisation process under low-potential control in alkaline molybdate solution has been used to modify the properties of the oxide film and in this way enhance the anticorrosion properties of the alloy. A dense and smooth surface has been achieved using this method, which does not present microcracks or porous defects. The amount of Ni and Ti released into Ringer solution under OCP condition as well as at potentials where the bare substrate suffers pitting attack showed that the dissolution of the alloy was significantly reduced by the presence of the anodised oxide film.

The oxide grown potentiostatically consists mainly of TiO_2 with a small amount of nickel. The mole ratio of Ti/Ni on the outermost surface is drastically increased. The improvement in corrosion behaviour is attributed to an increase in TiO_2 content on the surface to form a new, stable and protective layer. Moreover, the presence of molybdenum oxide species on the anodised film also contributes to improve the corrosion resistance.

Electrochemical results and quantitative analysis of the Ringer solution indicate that this anodisation technique can be easily used for future applications of the NiTi alloy.

Acknowledgments

The financial support of the Secretaría de Ciencia y Técnica - UNS (PGI 24/M127), the Consejo Nacional de Investigaciones Científicas y Técnicas (CONICET- PIP 112-201101-00055) and the Agencia Nacional de Promoción Científica y Tecnológica (ANPCYT PICT-2012-0141) is gratefully acknowledged.

References

[1] S.M. Toker, D. Canadinc, H.J. Maier, O. Birer, Evaluation of passive oxide layer formation-biocompatibility relationship in NiTi shape memory alloys: geometry and body location dependency, Mater. Sci. Eng. C 36 (2014) 118–129.
[2] S. Shabalovskaya, J. Anderegg, J. Van Humbeeck, Critical overview of Nitinol surfaces and their modifications for medical applications, Acta Biomater. 4 (2008) 447–467.
[3] P. Shi, F.T. Cheng, H.C. Man, Improvement in corrosion resistance of NiTi by anodisation in acetic acid, Mater. Lett. 61 (2007) 2385–2388.
[4] F.T. Cheng, P. Shi, G.K.H. Pang, M.H. Wong, H.C. Man, Microstructural characterization of oxide film formed on NiTi by anodisation in acetic acid, J. Alloy Compd. 438 (2007) 238–242.
[5] N. Bayat, S. Sanjabi, Z.H. Barber, Improvement of corrosion resistance of NiTi sputtered thin films by anodisation, Appl. Surf. Sci. 257 (2011) 8493–8499.

[6] C. Yang, F. Chen, S. Chen, Anodisation of the dental arch wires, Mater. Chem. Phys. 100 (2006) 268–274.
[7] J. Kawakita, M. Stratmann, A.W. Hassel, High voltage pulse anodisation of a NiTi shape memory alloy, J. Electrochem. Soc. 154 (2007) C294–C298.
[8] J.W.J. Silva, E.N. Codaro, R.Z. Nakazato, L.R.O. Hein, Influence of chromate, molybdate and tungstate on pit formation in chloride medium, Appl. Surf. Sci. 252 (2005) 1117–1122.
[9] A.M. Shams El Din, R.A. Mohammed, H.H. Haggag, Corrosion inhibition by molybdate/polymaliate mixtures, Desalination 114 (1997) 85–95.
[10] S. Maximovitch, G. Barral, F. Le Cras, F. Claudet, S. Maximovitch, The electrochemical incorporation of molybdenum in the passive layer of a 17% Cr ferritic stainless steel. Its influence on film stability in sulphuric acid and on pitting corrosion in chloride media, Corros. Sci. 37 (1995) 271–291.
[11] K.C. Emregül, A.A. Aksüt, The effect of sodium molybdate on the pitting corrosion of aluminum, Corros. Sci. 45 (2003) 2415–2433.
[12] X. Li, S. Deng, H. Fu, Sodium molybdate as a corrosion inhibitor for aluminium in H_3PO_4 solution, Corros. Sci. 53 (2011) 2748–2753.
[13] C.T. Kwok, Laser Surface Modification of Alloys for Corrosion and Erosion Resistance (Part 1), 2012.
[14] G.T. Burstein, C. Liu, R.M. Souto, The effect of temperature on the nucleation of corrosion pits on titanium in Ringer's physiological solution, Biomater 26 (2005) 245–256.
[15] J.F. Ziegler, J.P. Biersack, SRIM-2013, the Stopping and Range of Ions in Matter, code available in, http://www.srim.org.
[16] D. Velten, V. Biehl, F. Aubertin, B. Valeske, W. Possart, J. Breme, Preparation of TiO_2 layers on cp-Ti and Ti6Al4V by thermal and anodic oxidation and by sol-gel coating techniques and their characterization, J. Biomed. Mater. Res. 59 (2002) 18–28.
[17] V. Moutarlier, M.P. Gigandet, L. Ricq, J. Pagetti, Electrochemical characterisation of anodic oxidation films formed in presence of corrosion inhibitors, Appl. Surf. Sci. 183 (2001) 1–9.
[18] X. Su, T. Wang, W. Hao, L. He, Electrolytic passivation of nitinol shape memory alloy in different electrolytes, Chin. J. Aeronaut. 19 (2006) S113–S118.
[19] C. Cheng-lin, H. Tao, S.L. Wu, W. Ru-meng, D. Yin-sheng, L. Ping-hua, C.Y. Chung, P.K. Chu, In situ synthesis of nanostructured titania film on NiTi shape memory alloy by Fenton's oxidation method, Trans. Nonferr. Met. Soc. China 17 (2007) 902–906.
[20] I. Milosev, B. Kapun, The corrosion resistance of Nitinol alloy in simulated physiological solutions Part 2: the effect of surface treatment, Mater. Sci. Eng. C 32 (2012) 1068–1077.
[21] J.F. Moulder, Handbook of X-ray Photoelectron Spectroscopy: a Reference Book of Standard Spectra for Identification and Interpretation of XPS Data, 1992.
[22] J. Yeh, I. Lindau, Atomic and Nuclear Data Tables, 32, 1985, pp. 1–155.
[23] N.S. Mc Intyre, D.D. Johnston, L.L. Coatsworth, R.D. Davidson, J.R. Brown, Surf. Interface Anal. 15 (1990) 265–272.